



#### Available online at www.sciencedirect.com

# **ScienceDirect**

Procedia Structural Integrity 68 (2025) 1216-1222



European Conference on Fracture 2024

# Mixed mode fracture toughness of R260Mn rail steel using Compact Tension Shear specimens

Sjoerd T. Hengeveld<sup>a,b,\*</sup>, Davide Leonetti<sup>a</sup>, H.H. (Bert) Snijder<sup>a</sup>, Johan Maljaars<sup>a,b</sup>

<sup>a</sup>Structural Engineering and Design, Eindhoven University of Technology, De Zaale 1, Eindhoven 5612 AZ, The Netherlands
<sup>b</sup>Reliable Structures, TNO, Molengraaffsingel 8, Delft 2629 JD, The Netherlands

#### **Abstract**

Being able to describe the fracture condition of a railway rail, after a fatigue crack has initiated, is crucial for safety assessment. Rails are loaded in mixed mode. This paper concerns an experimental investigation into the mixed-mode fracture toughness of used R260Mn rail steel. Fracture toughness experiments are carried out using compact tension shear specimens. This setup allows for testing fracture in mixed mode load condition (Mode-I and Mode-II). Results are compared in terms of maximum equivalent and maximum Mode-I fracture toughness. Contrary to the commonly adopted mixed mode failure criterion of Richard (Richard et al. (2004)) it appears that mixed mode failure is best described by the maximum Mode-I stress intensity factor component for the steel grade of study. The average fracture toughness of 51 MPa  $\sqrt{m}$  is obtained, for 10 mm thick specimens.

© 2025 The Authors. Published by ELSEVIER B.V.
This is an open access article under the CC BY-NC-ND license (https://creativecommons.org/licenses/by-nc-nd/4.0)
Peer-review under responsibility of ECF24 organizers

Keywords: Fracture toughness; Mixed mode fracture; rail steel

#### 1. Introduction

Accurately describing the fatigue crack growth rate, the fatigue crack growth direction and failure condition are crucial for determining the residual fatigue life of steel structures in general and thus also for railway rails, Zerbst et al. (2009). Squats are complex crack networks formed due to rolling contact fatigue, originating from the head of the rail, growing downwards. They are often decisive for maintenance, Magel et al. (2016). The wheel-rail contact results in a multi-axial stress state in the vicinity of the squat. The stress intensity factor (SIF) is often considered as crack driving force for determining the failure condition. It depends on the applied load, the crack length, and the geometry. The failure condition in rail steel is often governed by cleavage (brittle) fracture. Fracture toughness is the material property used to estimate the onset of brittle fracture. This fracture toughness can be mode-dependent, Richard et al. (2004). Most studies on rail steel focus on the determination of Mode-I fracture toughness, I. Vitez (1993); Christodoulou et al. (2016); Ravaee and Hassani (2007). Mode-I fracture toughness is usually determined using standardized specimens

<sup>\*</sup> Corresponding author E-mail address: s.t.hengeveld@tue.nl

such as Single Edge Notched Bending, SE(B) specimen or Compact Tension C(T) specimen (e.g. ASTM E399, ASTM (2020)). However, for mixed mode fracture toughness this standardization is lacking. Banks-Sills L. (1986) developed a specimen specifically for Mode-II testing, initially developed to determine the fracture toughness of Plexiglass. Afterwards, they showed its potential in determining the Mode-II fracture toughness of metals, Banks-Sills (1989). Richard (1984) extended this setup from pure Mode-II loading to mixed Mode-I and Mode-II loading, developing the compact tension shear (CTS) specimen and a mixed mode set-up. Several researchers used variants of his experimental set-up to measure the mixed mode fracture toughness, Miao et al. (2018); Hallbäck (1997) or mixed mode fatigue crack growth rate Lesiuk et al. (2020); Peixoto and de Castro (2016). Its wide application is CTS.

In the current paper, mixed-mode fracture toughness experiments are reported using CTS specimen. The specimens are created from R260Mn used rails.

#### 2. Material characterization

The specimens used in the current study were extracted from used railway rails, manufactured between 1991 and 2005. These tracks are mixed (cargo and passenger) tracks with an annual transported mass between  $7 \times 10^9$  kg and  $11 \times 10^9$  kg. The samples are extracted in the vicinity of a squat defect. The material is R260Mn, which is a commonly used rail steel in The Netherlands. Four cylindrical tensile test coupons are extracted from the head of the rails, see inset in Figure 1b. The tensile tests are done using an INSTRON 5958 electro-mechanical testing machine. The tests are conducted in displacement control with a constant speed of 0.01 mm/s. Table 1 shows the results. The third column gives the number of tests, the fourth column gives the mean Young's Modulus. The fifth and sixth column provide respectively the mean tensile strength and mean yield stress. The third row show results obtained from literature for rail steel R260, (Motameni and Eraslan (2016); Christodoulou et al. (2016); Nejad et al. (2019); I. Vitez (1993); Vitez et al. (2000)) and R260Mn I. Vitez (1993); Vitez et al. (2000).

Table 1: Monotonic properties of R260Mn Rail steel, mean values and standard deviation between brackets.

	condition	$n_{test}$	E[Gpa]	$\sigma_u[MPa]$	$\sigma_{ys}[MPa]$
Current research	used	4	211(5.1)	925(8)	571(3) <sup>c</sup>
Literature	new	19	_a	922(83)b	533(39) <sup>b,d</sup>

<sup>&</sup>lt;sup>a</sup> Not all sources provided E, so not taken into account in this comparsion.

The mean yield stress and mean tensile strength obtained in this study are compared to the values obtained in literature using a two-sample Z-test. This statistical test evaluates equality of mean values of different sets, assuming normal distributed sets. The two-tailed statistic for this test is the p-value. The p-value for equality of the mean values of the tensile strengths, p = 0.86, is larger than the significance level of 0.05 meaning there is not sufficient evidence that the mean values of experiments are different from literature. However, the experimentally obtained yield stress is significantly higher than the one obtained from literature as the p-value  $p = 4 \times 10^{-5}$  is lower than the assumed significance level of 0.05. A possible explanation for this difference is hardening, expected to have taken place in the head of the used rails examined in the current study. Hardening in the head of the rail takes place in operation, Zerbst et al. (2005). Most tests done in literature are done on newly fabricated rails.

# 3. Experimental program

# 3.1. Specimen design and experimental setup

The mixed-mode fracture toughness is determined using CTS specimens as shown in Figure 1a. The notch is created with a single pass of electrical discharge machining, resulting in a notch with a width of approximately 0.2 mm and a length of 23 mm. Figure 1b shows the extraction location of the specimen in the head of the rail. Figure 1d shows

<sup>&</sup>lt;sup>b</sup> For I. Vitez (1993) R260 individual results unknown, mean and range available ( $n_{test} = 4$ ).

<sup>&</sup>lt;sup>c</sup> Offset yield stress  $\sigma_{v,0.2}$ 

<sup>&</sup>lt;sup>d</sup> \(\sigma\_{y,0.2}\) for Christodoulou et al. (2016), Upper yield point \(R\_{eh}\) for I. Vitez (1993); Vitez et al. (2000). Unknown for Motameni and Eraslan (2016) and Nejad et al. (2019)

the complete CTS setup. The setup exists of two clevises, fabricated according to ASTM (2020) and connected to the hydraulic machine. Two CTS brackets are connected to this clevis. For this connection seven holes are provided. Fitting pins connect the CTS specimens to the brackets. The brackets has slots instead of holes, to create a statically determined system, Richard (1984). Figure 1c shows the hydraulic testing frame which a capacity of 400 kN and equipped with a 125 kN load cell.

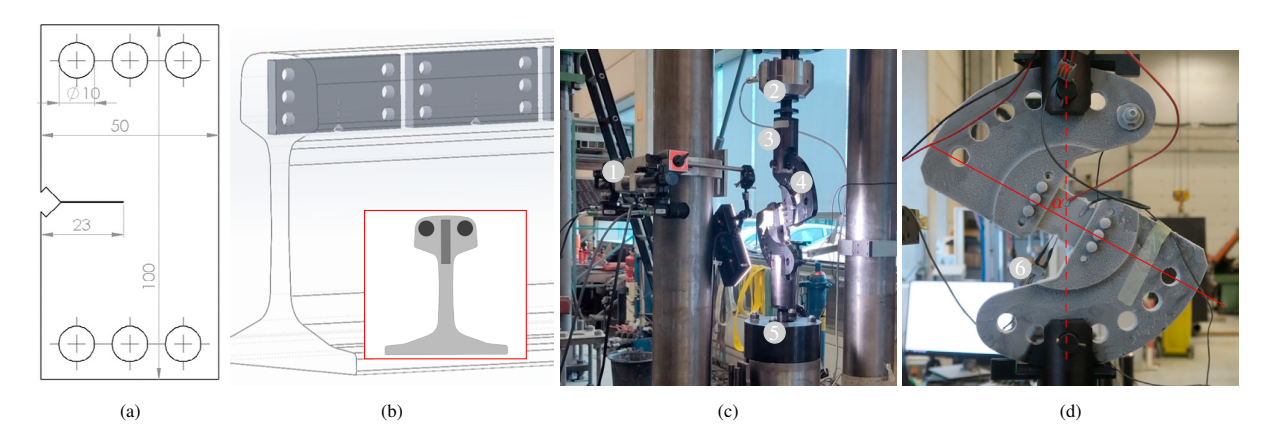


Fig. 1: Experimental setup to determine mixed mode fracture toughness: (a) CTS specimen with dimensions, all dimensions in mm, thickness 10 mm. (b) Position of specimens in rail (c) Hydraulic machine including CTS setup (1) Digital Image Correlation camera's (2) Load cell (3) Clevis (4) CTS bracket and specimen (5) Hydraulic actuator (d) Close-up of cooled CTS specimen and bracket and definition of loading angle  $\alpha$  (6) Clip extensometer.

Depending on the applied load angle,  $\alpha$ , a specific biaxiality ratio,  $\beta$ , between Mode-I ( $\alpha = 0^{\circ}$ ) and Mode-II ( $\alpha = 90^{\circ}$ ) is applied to the specimen. The SIF as function of the load angle is obtained from Jin et al. (2022):

$$Y_{I}(\alpha, a) = \left[1.57334 - 0.42443 \left(\frac{a}{w}\right) - 0.03252 \left(\frac{a}{w}\right)^{2} + 5.02089 \left(\frac{a}{w}\right)^{3} + 15.79799 \left(\frac{a}{w}\right)^{4}\right] \cos \alpha$$

$$Y_{II}(\alpha, a) = \left[0.48915 + 1.32188 \left(\frac{a}{w}\right) + 1.24338 \left(\frac{a}{w}\right)^{2} - 0.076993 \left(\frac{a}{w}\right)^{3}\right] \sin \alpha$$

$$\beta(\alpha, a) = \frac{Y_{II}(\alpha, a)}{Y_{I}(\alpha, a)}, \quad K_{I}(\alpha, a, F) = \frac{F\sqrt{\pi a}}{wt} Y_{I}(\alpha, a), \quad K_{II}(\alpha, a, F) = \frac{F\sqrt{\pi a}}{wt} Y_{II}(\alpha, a)$$
(1)

In which a is the crack length in mm, F is the applied load in N, and w and t are respectively the specimen width and thickness both in mm. A commonly used definition of the equivalent SIF is the one by Richard et al. (2004).

$$Y_{eq}(\alpha, a) = \frac{Y_{I}(\alpha, a)}{2} + \frac{1}{2} \sqrt{Y_{I}(\alpha, a)^{2} + 4 \left[c_{1} Y_{II}(\alpha, a)\right]^{2}}, \quad K_{eq}(\alpha, a, F) = \frac{F \sqrt{\pi a}}{wt} Y_{eq}(\alpha, a)$$
 (2)

This definition of equivalent SIF is formulated in a similar way as the Von Mises equivalent stress. The material constant  $c_1$  is set to 1.155, independent of the material.

Fracture toughness depends on the crack-tip constraint, which is a function of the specimen geometry, the crack size and the loading condition. The plane-strain fracture toughness is defined as a geometrically independent lower limit of the fracture toughness. Therefore the standards prescribe the minimum specimen dimensions to ensure a plane strain condition. These limits are developed for Mode-I testing. As the focus is on mixed-mode fracture toughness, these limits are not taken into account.

## 3.2. Experimental test phases

All experiments are divided in three phases, namely, a pre-cracking phase, a mixed mode compliance loading phase and the final fracture phase.

During the pre-cracking phase the initial notch is extended to a fatigue crack in order to create a sharp notch. This fatigue crack is created in Mode-I ( $\alpha=0$ ) with a stress ratio R=0.1. The SIF range at the final pre-crack length is shown in Table 2. The crack extension is monitored using a crack gauge with an interval of 0.1 mm (KYOWA KV-5C). Whenever the crack grows through a single wire of the crack gauge, a jump in measured strain of approximately 35  $\mu\epsilon$  is seen. Next to this, the CMOD is monitored using a clip extensometer. A pre-crack frequency between 8 Hz and 14 Hz is used depending on the applied load.

In the second phase the specimens are loaded in mixed mode up to an equivalent pre-crack load,  $F_{eq}$  at room temperature. During this phase digital image correlation (DIC) is used to evaluate the mixed-mode displacements. The DIC is used to measure the crack mouth opening displacement (CMOD), the crack mouth sliding displacement (CMSD) and thereby the crack mouth total displacement (CMTD), which is advantageous compared to the clip extensometer that only measures the CMOD. The equivalent pre-crack SIF,  $K_{eq,pc}$  is defined in such a way that it does not exceed the maximum  $K_I$  applied at the end of the pre-crack phase, corresponding to a crack length  $a_{pc}$  and a maximum load,  $F_{pc}^{max}$ :  $K_{eq,pc}\left(\alpha, a_{pc}, F_{pc}^{max}\right) < K_I\left(0, a_{pc}, F_{pc}^{max}\right)$ . The DIC system exists of two camera's (12 MP, 50 mm lens). Using spray paint, a speckle pattern is applied to the specimens to accommodate DIC.

Finally the specimens are fractured. The goal of this experimental campaign is to do the fracture tests at approximately -5 °C. To accomplish this, both specimen and the brackets were cooled down to approximately -40 °C. After this the setup was moved out of the fridge and inserted in the hydraulic testing machine. The temperature was monitored during cooling and installation in the hydraulic machine, using thermocouples on both the specimen and on one bracket. The thermocouple on the specimen was glued to the back face. To enhance the heat transfer from the specimen to the thermocouple, a layer of cooling paste was added. The fracture test was started when the thermocouple on the specimen measured -6 °C. The fracture tests were done in load control with an approximate loading rate of  $K_{eq} = 2 \text{ MPa } \sqrt{\text{m}} \text{ (ASTM (2020))}$ . The applied load, the displacement of the cylinder and the measured CMOD of extensometer were recorded during the test with a measurement frequency of 1000hz. Due to condensation it was not possible to use the DIC system during the fracture phase.

#### 4. Results

The current research exists of 13 tests, the results of three experiments are discussed in detail in this paper, two in pure Mode-I loading and a one mixed mode experiment with  $\alpha = 45^{\circ}$ . Figure 3 shows the load displacement curves of the three tests. The displacement u is the CMOD displacement measured by the clip extensometer. The blue curve shows the experimental data, smoothed with a moving average filter with a window width of n = 25 samples. The solid black line is the best fitted line through the initial linear part following the procedure as described in the ASTM E399.

## 4.1. Specimen C-1

Figure 3a shows the results for specimen C-1, a pure Mode-I test ( $\alpha = 0^{\circ}$ ). Three region's can be observed, in the experimental load-displacement curve, namely, an initial part at  $0 \,\mathrm{kN} < F < 11 \,\mathrm{kN}$  a linear part in the interval  $11 \,\mathrm{kN} < F < 26.5 \,\mathrm{kN}$  at which a small pop-in is visible. Finally, the third, a linear part between pop-in and final fracture at  $32.5 \,\mathrm{kN}$ .

The change in stiffness between the first and second part is a consequence of crack closure. Due to pre-cracking, plasticity develops in the vicinity of the crack-tip and in the wake of the crack. The crack closure is estimated using Newman's crack closure model, (Newman (1984)) with the maximum applied pre-crack load  $F_{pc} = 15 \,\mathrm{kN}$ . This results in an opening load between  $4 \,\mathrm{kN}$  and  $8.1 \,\mathrm{kN}$  depending on a plane strain or the plane stress assumption. This is lower than the  $11 \,\mathrm{kN}$  measured in this experiment, which would indicate other sources of crack-closure. Evaluating the fracture surfaces shows a relative rough surface, which gives evidence to roughness induced crack closure (RICC). This is also seen in literature for other rail steels, Bonniot et al. (2018).

A pop-in is a sudden (brittle) crack extension after which the crack arrests. A discontinuity in the CMOD of approximately 0.05 mm is seen in the experiment. The load displacement curve after pop-in is again approximately linear, but with a lower slope than before pop-in, due to the lower stiffness caused by the crack extension.

Figure 2 shows the fracture surface. Three regions can clearly be distinguished, namely, the initial notch, the relatively smooth pre-crack region, and the brittle fracture surface. The fatigue crack growth was slightly asymmetric. However, as the total crack length is the initial notch plus the pre-crack length, this is assumed to not affect the fracture toughness determination. The crack length of specimen C-1 varies between 24.4 mm and 25.4 mm and it is 25 mm on average. Using Equation 2 and the fracture load, an equivalent maximum SIF  $K_{eq}^{max} = 54$  MPa  $\sqrt{m}$  is determined.

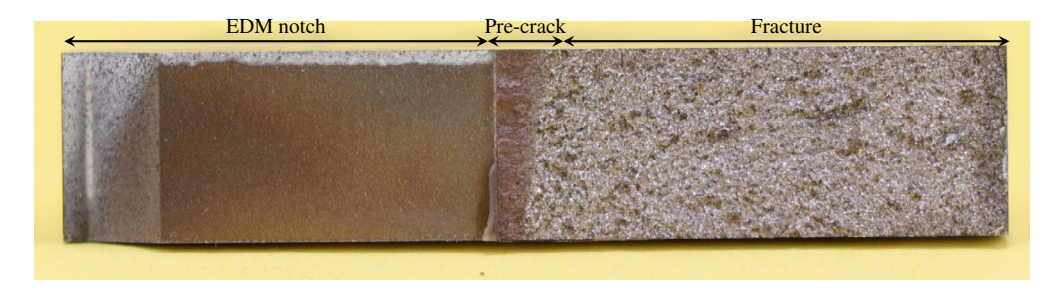


Fig. 2: Fracture surface specimen C-1.

# 4.2. Specimen C-2

Figure 3b shows the results of the second specimen, which is also a pure Mode-I test. Again, three different regions can be distinguished. The opening load appears to be similar to the one of Experiment C-1. At approximately 29 kN a pop-in occurs with a displacement jump of approximately 0.1 mm. After the pop-in, only a small increase of the load leads to complete failure of the specimen. The final fracture load is 39.8 kN which, in combination with a measured crack length of 25.3 mm, corresponds to  $K_{eq}^{max} = 53$  MPa  $\sqrt{m}$ .

# 4.3. Specimen C-3

Figure 3c shows the results of the third specimen. This is a specimen loaded under a load angle  $\alpha=45^{\circ}$ . Again the curved blue line represents the experiment, the black solid line is a straight line through the linear part of the experimental curve, and the red curve is the signal measured by the crack-gauge during the fracture test, for which the horizontal axis at the top of the graph should be used. When unloading the specimen between the pre-cracking phase and the fracture test, the wires of the crack gauges are partly in contact, leading to an inaccurate reading of the strain output. When reaching the equivalent crack opening load, the wires disconnect, and crack-growth can be measured again. This equivalent load  $F_{pc,eq}$  is determined with:

$$F_{pc,eq} = \frac{Y_I(0,a)}{Y_I(45,a)} F_{pc,max}$$
 (3)

in which,  $F_{pc,max}$  is the maximum applied load during the pre-cracking phase. This equivalent load is indicated with the red dot in the curve. Three regions are observed in the experimental load displacement curve, namely, a curved part between 0 kN and 8 kN, a straight part between 8 kN and 25 kN, and a curved part between 25 kN and 3.9 kN. The first, crack closure influenced part, is not so distinctive as for the Mode-I tests. From approximately 28 kN onwards the crack gauge indicates crack extension. This crack extension is not visible in the load displacement curves in terms of pop-ins. The final fracture load is 37.9 kN, which corresponds to  $K_{eq,max} = 60 \text{ MPa } \sqrt{\text{m}}$ .

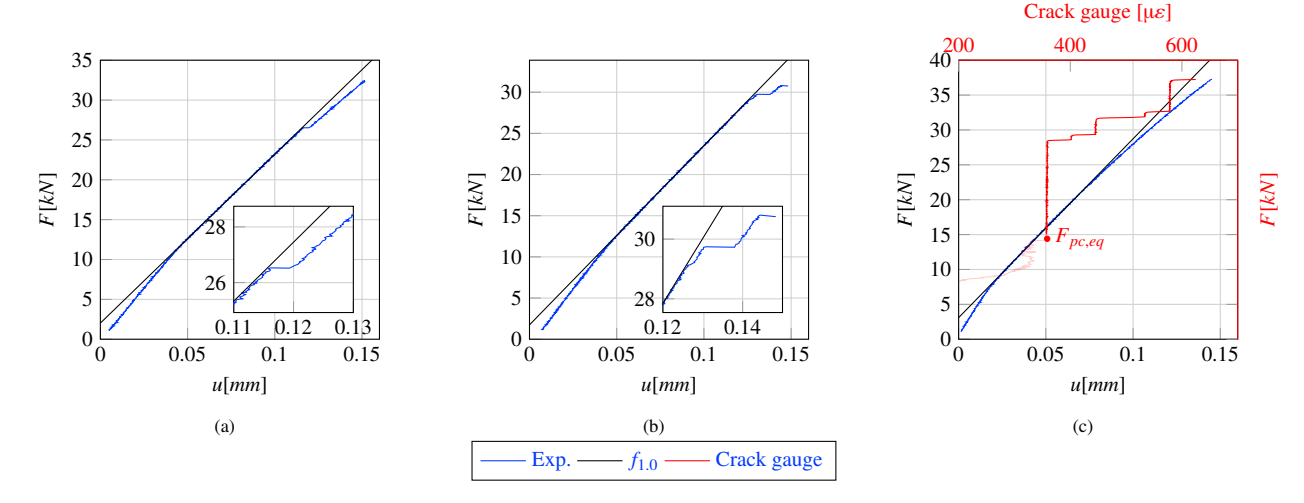


Fig. 3: Load displacement curves of fracture test: (a) Specimen C-1,  $\alpha = 0^{\circ}$  (b) Specimen C-2,  $\alpha = 0^{\circ}$  (c) Specimen C-3  $\alpha = 45^{\circ}$ .

# 4.4. Overview

Table 2 shows a summary of the fracture results. The first columns give the specimen name, the applied load angle, and the corresponding biaxiality. The fourth column provides the pre-crack length. The fifth column shows the maximum SIF at the end of the pre-crack phase. The sixth column gives the load at complete fracture. The seventh column is the equivalent SIF, see Equation 2, at the fracture load. The last column is the Mode-I SIF at fracture. The last row gives the mean fracture toughness as well the standard deviation (between brackets). The goal of this research is to determine the final fracture load. Pop-ins are not taken into account in the evaluation, contrary to the procedure as described in the E399.

specimen  $K_{I,pc,max}$   $\overline{[MPa \sqrt{m}]}$  $F^{max}$  [kN]  $K_{eq}^{max}$  [MPa  $\sqrt{m}$ ]  $[MPa \sqrt{m}]$  $\beta [-]$ a [mm]α [°] C-1 25.0 25 0 0.0 32.5 54.0 54.0 C-2 26 0 0.0 25.3 30.9 52.9 52.9 C-3 49.8 45 0.43 18 37.3 60.0 26.3 mean(std.) 55.6(3.8) 52.2(2.2)

Table 2: Summary of fracture test results

Specimens C-1 and C-2 result in a similar SIF. Both show a pop-in. Specimen C-3 has a higher equivalent SIF at fracture than the other two specimens, whereas the Mode-I SIFs at fracture of the three tests are more aligned. This is shown here for one mixed mode specimen only, but the same trend is observed for all specimens in the test program. The mean  $K_I^{max}$  for all tests is 51.4 MPa  $\sqrt{m}$  with a standard deviation of 5.5 MPa  $\sqrt{m}$  and the  $K_{eq}^{max}$  is 58 MPa  $\sqrt{m}$  with a standard deviation of 9.8 MPa  $\sqrt{m}$ . The non-linear behaviour in the final region of Specimen C-3 could be an indication that plasticity occurs around the crack-tip and that characterization of the fracture behaviour using linear elastic fracture mechanics (LEFM) is no longer valid. A CTOD type of evaluation might be more suited, Wells (1963).

As these fracture results are thickness dependent, a direct comparison with fracture toughness values from similar steels reported in literature is not possible.

#### 5. Conclusions and recommendations

This paper presents the mixed mode fracture toughness characterization of R2560Mn rail steel. Monotonic tensile tests are carried out to determine the yield and ultimate stress. The ultimate stress is in line with literature and the yield stress is slightly higher, possibly caused by strain hardening during operation of the rails. Mixed-mode fracture toughness tests have been done using CTS specimen at -5 °C. These fracture toughness values are valid for CTS

specimen with a thickness of 10 mm. Evaluation of the results shows that the final fracture is described better by the Mode-I SIF than by the equivalent SIF. The tests resulted in an average fracture toughness of 51 MPa  $\sqrt{m}$  with a coefficient of variation of 0.11.

# Acknowledgements

This research was carried out under project number T20008 in the framework of the Research Program of the Materials innovation institute (M2i) (www.m2i.nl) supported by the Dutch government. The Dutch railway asset owner ProRail is acknowledged for its contribution to this research.

#### References

- ASTM, 2020. E399-20a Standard Test Method for Linear-Elastic Plane-Strain Fracture Toughness of Metallic Materials. Technical Report. ASTM International. doi:10.1520/e0399-23.
- Banks-Sills, L., 1989. Application of a mode ii fracture specimen to plastically deforming material, in: KHAN, A.S., TOKUDA, M. (Eds.), Advances in Plasticity 1989. Pergamon, Oxford, pp. 483-486. URL: https://www.sciencedirect.com/science/article/pii/B9780080401829501193, doi:https://doi.org/10.1016/B978-0-08-040182-9.50119-3.
- Banks-Sills L., A.M., 1986. A compact mode ii fracture specimen, in: Fracture Mechanics: Seventeenth Volume, ASTM International100 Barr Harbor Drive, PO Box C700, West Conshohocken, PA 19428-2959. pp. 347–363. doi:10.1520/STP17406S.
- Bonniot, T., Doquet, V., Mai, S.H., 2018. Mixed mode II and III fatigue crack growth in a rail steel. International Journal of Fatigue 115, 42-52. doi:10.1016/j.ijfatigue.2018.01.010.
- Christodoulou, P., Kermanidis, A., Haidemenopoulos, G., 2016. Fatigue and fracture behavior of pearlitic grade 900a steel used in railway applications. Theoretical and Applied Fracture Mechanics 83, 51–59. doi:10.1016/j.tafmec.2015.12.017.
- Hallbäck, N., 1997. Mixed-mode i/ii fracture behaviour of a high strength steel. International Journal of Fracture 87, 363–388. doi:10.1023/a: 1007448511822.
- I. Vitez, B.T., 1993. Importance of knowning fracture toughness and fatigue strength of railway rails, in: Reliability and Structural Integrity of Advanced Materials, pp. 1291–1296.
- Jin, P., Liu, Z., Wang, X., Chen, X., 2022. Three-dimensional analysis of mixed mode compact-tension-shear (CTS) specimens: Stress intensity factors, t-stresses and crack initiation angles. Theoretical and Applied Fracture Mechanics 118, 103218. doi:10.1016/j.tafmec.2021. 103218.
- Lesiuk, G., Smolnicki, M., Mech, R., Zięty, A., Fragassa, C., 2020. Analysis of fatigue crack growth under mixed mode (i + II) loading conditions in rail steel using CTS specimen. Engineering Failure Analysis 109, 104354. doi:10.1016/j.engfailanal.2019.104354.
- Magel, E., Mutton, P., Ekberg, A., Kapoor, A., 2016. Rolling contact fatigue, wear and broken rail derailments. Wear 366-367, 249–257. doi:10.1016/j.wear.2016.06.009.
- Miao, X.T., Yu, Q., Zhou, C.Y., Li, J., Wang, Y.Z., He, X.H., 2018. Experimental and numerical investigation on fracture behavior of CTS specimen under i-II mixed mode loading. European Journal of Mechanics A/Solids 72, 235–244. doi:10.1016/j.euromechsol.2018.04.019.
- Motameni, A., Eraslan, A.N., 2016. Fracture and fatigue crack growth characterization of conventional and head hardened railway rail steel. Journal of Scientific and Engineering Research, 367–376.
- Nejad, R.M., Shariati, M., Farhangdoost, K., 2019. Prediction of fatigue crack propagation and fractography of rail steel. Theoretical and Applied Fracture Mechanics 101, 320–331. doi:10.1016/j.tafmec.2019.03.016.
- Newman, J.C., 1984. A crack opening stress equation for fatigue crack growth. International Journal of Fracture 24, R131–R135. doi:10.1007/bf00020751.
- Peixoto, D.F., de Castro, P.M., 2016. Mixed mode fatigue crack propagation in a railway wheel steel. Procedia Structural Integrity 1, 150–157. doi:10.1016/j.prostr.2016.02.021.
- Ravaee, R., Hassani, A., 2007. Fracture mechanics determinations of allowable crack size in railroad rails. Journal of Failure Analysis and Prevention 7, 305–310. doi:10.1007/s11668-007-9068-7.
- Richard, H., 1984. Some theoretical and experimental aspects of mixed mode fractures, in: Fracture 84. Elsevier, pp. 3337–3344. doi:10.1016/b978-1-4832-8440-8.50358-6.
- Richard, H.A., Fulland, M., Sander, M., 2004. Theoretical crack path prediction. Fatigue & Fracture of Engineering Materials & Structures 28, 3–12. doi:10.1111/j.1460-2695.2004.00855.x.
- Vitez, I., Krumes, D., Budić, I., Haračić, N., 2000. Contribution to the correlation between fatigue endurance and tensile strength of steel. Mašinstvo, ISSN 1512-5173 4, 161–170.
- Wells, A., 1963. Application of fracture mechanics at and beyond general yielding. British Welding Journal 10.
- Zerbst, U., Lunden, R., Edel, K.O., Smith, R., 2009. Introduction to the damage tolerance behaviour of railway rails a review. Engineering Fracture Mechanics 76, 2563–2601. doi:10.1016/j.engfracmech.2009.09.003.
- Zerbst, U., Mädler, K., Hintze, H., 2005. Fracture mechanics in railway applications—an overview. Engineering Fracture Mechanics 72, 163–194. doi:10.1016/j.engfracmech.2003.11.010.